Simple model for the vibrations of embedded elastically cubic nanocrystals

Lucien Saviot,[1,*] Daniel B. Murray,[2,†] Eugène Duval,[3] Alain Mermet,[3]
Sergey Sirotkin,[3] and María del Carmen Marco de Lucas[1]
[1]*Laboratoire Interdisciplinaire Carnot de Bourgogne, UMR 5209 CNRS, Université de Bourgogne, 9 Av. A. Savary, BP 47 870, F-21078 Dijon Cedex, France*
[2]*Department of Physics, University of British Columbia Okanagan, 3333 University Way, Kelowna, British Columbia, Canada V1V 1V7*
[3]*Laboratoire de Physico-Chimie des Matériaux Luminescents, Université de Lyon–Université Claude Bernard Lyon 1, UMR 5620 CNRS, 69622 Villeurbanne, France*
(Received 21 July 2010; published 28 September 2010)

The purpose of this work is to calculate the vibrational modes of an elastically anisotropic sphere embedded in an isotropic matrix. This has important application to understanding the spectra of low-frequency Raman scattering from nanoparticles embedded in a glass matrix. First some low-frequency vibrational modes of a free cubically elastic sphere are found to be nearly independent of one combination of elastic constants. This is then exploited to obtain an isotropic approximation for these modes which enables to take into account the surrounding isotropic matrix. This method is then used to quantitatively explain recent spectra of gold and copper nanocrystals in glasses.

DOI: 10.1103/PhysRevB.82.115450 PACS number(s): 63.22.Kn

I. INTRODUCTION

Low-frequency inelastic light scattering by metallic nanoparticles, which is due to their mechanical vibrations, has been the focus of attention of many researchers during the last 30 years.[1–4] This scattering is similar to surface-enhanced Raman scattering from molecules close to such a metallic nanostructure[1] making it an interesting complementary way to study this complex phenomenon having many applications for very sensitive detection. The enhancement due to using laser excitations resonant with the dipolar plasmon in such nanostructures and the high-quality samples available today are responsible for low-frequency Raman spectra having an unmatched number of features[5] compared to nonmetallic nanoparticles.

The interpretation of such spectra is very challenging as many parameters have to be taken into account at the same time. The mechanical vibrations depend on the shape of the nanoparticles but also on their inner structure and on the surrounding medium. In this work, we report on an approach enabling taking into account all these parameters for a spherical nanoparticle having a cubic lattice embedded in a glass matrix.

The vibrational modes of an elastically isotropic sphere which is free[6] or embedded in an infinite isotropic matrix[7,8] are known exactly. When the elastic constants are not isotropic, a numerical approach such as the one known as resonant ultrasound (RUS) (Ref. 9) can find mode frequencies and displacement fields of free nanoparticles.[10–12] What has been missing up until now is a description of the vibrations of an elastically anisotropic sphere embedded in an isotropic matrix. The case of anisotropic elasticity has been discussed for the problem of the scattering of acoustic waves[13,14] but none of these approaches provides the eigendisplacements required for modeling the coupling of the vibrations with electrons which is at work in all the optical techniques used to detect such vibrations.

Current experimental results such as those presented in Ref. 5 have already shown the need for a model without any of these limitations. The interpretation in that paper took into account the elastic anisotropy to qualitatively explain the splitting of the lowest frequency Raman peaks but it failed to provide a quantitative description due to the significant coupling with the embedding matrix. The present work fills that hole by showing that it is possible to choose an isotropic approximation of the system for the most intense Raman-active vibrations which enables the prediction of the position of the Raman peaks and provides the vibrational displacement fields required for the calculation of the Raman intensities.

II. METHOD

Exact solutions for the vibrations of isotropic free spheres can be classified as spheroidal and torsional and will be noted $S^n_{\ell,m}$ and $T^n_{\ell,m}$, respectively, in the following with ℓ and m being the usual angular momentum and its z component and n being an index used to label the eigenmodes by increasing frequency starting from $n=1$ as in a previous work.[12] For spheres whose diameter is small compared to the wavelength of light, the Raman-active vibrations are S_0 and S_2 (for every m and n).[15] In the present work, RUS calculations have been used to model the vibrations of elastically anisotropic spheres as in a previous work[12] by expanding the displacements onto $x^i y^j z^k$ functions with $i+j+k \leq 20$.

The approach of this paper was inspired by the calculations for elastically anisotropic cuboctaedra in Ref. 16. The idea was to calculate mode frequencies using only the speed of sound along a single propagation direction. The fivefold degenerate S^1_2 modes of an isotropic sphere are split by cubic elasticity into two degenerate modes with E_g symmetry and three with T_{2g} symmetry (O_h point group). Due to the symmetry of the displacements of the E_g and T_{2g} vibrations, their frequencies were approximated using sound speeds in particular directions instead of three-dimensional (3D)-averaged ones. It should be noted that all the E_g and T_{2g} vibrations (as well as the A_{1g} vibrations) are Raman active but only the

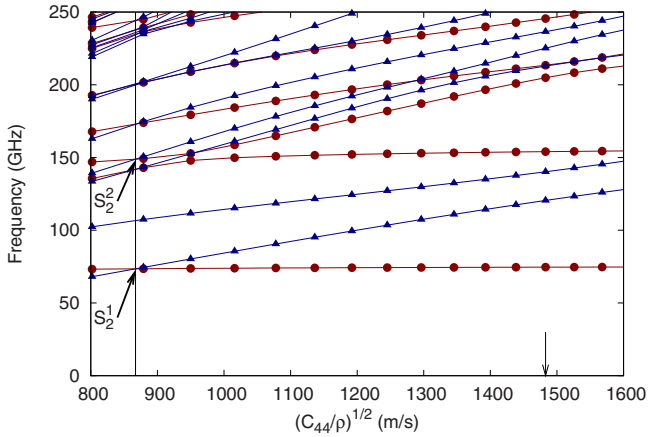

FIG. 1. (Color online) Variation in the eigenfrequencies of the lowest frequency E_g (circles, red) and T_{2g} (triangles, blue) vibrations of a gold sphere of radius 5 nm when varying C_{44}. The vertical arrow indicates the real abscissa for gold and the vertical line corresponds to an isotropic system.

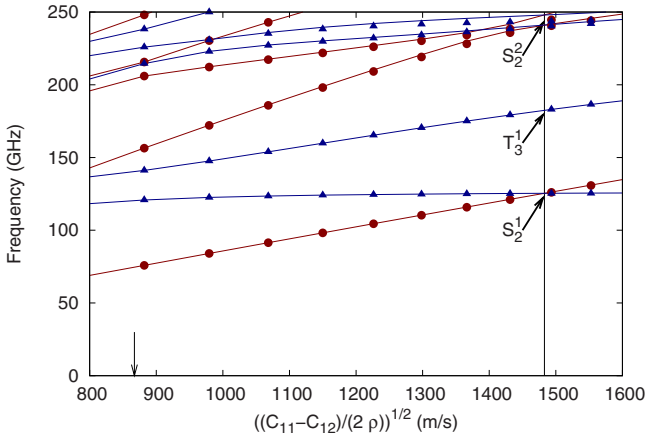

FIG. 2. (Color online) Variation in the eigenfrequencies of the E_g (circles for varying C_{12} and lines going through the circles for varying C_{11}, red) and T_{2g} (triangles for varying C_{12} and lines going through the triangles for varying C_{11}, blue) vibrations of a gold sphere of radius 5 nm as a function of $C_{11}-C_{12}$. The vertical arrow indicates the real abscissa for gold and the vertical line corresponds to an isotropic system.

ones sharing a strong similarity with the S_2 modes are expected to contribute significantly to the Raman spectra due to the surface-deformation scattering mechanism.[4]

In order to confirm the validity of this simple approach for spherical nanoparticles, we use a method similar to the one used in a previous work.[17] Studying the frequency changes resulting from a continuous variation in the elasticity of the material the sphere is made of provides some insight into the nature of the vibrations. A cubic material has three independent elastic constants C_{11}, C_{12}, and C_{44} instead of two for isotropic elasticity for which $C_{44}=\frac{C_{11}-C_{12}}{2}$. We consider the case of gold nanoparticles because of available inelastic light-scattering experimental data to compare with and also because gold has a very strong elastic anisotropy making it a good system to test the validity of the isotropic approximations. We use the following parameters: $C_{11}=191$ GPa, $C_{12}=162$ GPa, and $C_{44}=42.4$ GPa and mass density $\rho=19.283$ g cm^{-3}. Since we are mainly interested in Raman-active vibrations, we will focus on the vibrations coming from the isotropic S_2^1 mode which are the main features in the low-frequency Raman spectra of gold nanoparticles.

The potential for a great simplification in handling these modes, at least in some cases, can be clearly seen as follows. We plot eigenfrequencies for a gold sphere as a function of C_{44} in Fig. 1, instead of leaving C_{44} fixed at its normal value for gold. The two lowest frequency E_g branches, i.e., the fundamental mode and first overtone, are very nearly flat. The frequency change for the lowest E_g branch is 2% while C_{44} is multiplied by 4. This indicates that the corresponding modes approximately do not depend on C_{44} or the associated transverse sound speed. This approximate flatness is essential to our approach. In practice, it only holds very well for the lowest frequency modes and successively less well for higher frequency. The projection of the displacements[12] of the two lowest frequency E_g vibrations obtained for $\sqrt{C_{44}/\rho}=1600$ m/s onto those obtained for $\sqrt{C_{44}/\rho}=800$ m/s is very close to 1 ($\simeq 0.9968$). This demonstrates that the displacement field of these modes do not significantly change with C_{44} either. Since the mode approximately does not depend on C_{44}, we are free to arbitrarily change C_{44} to a different value which is convenient for us. Specifically, we can always choose C_{44} to change the gold into an isotropic material, i.e., $C_{44}=\frac{C_{11}-C_{12}}{2}$.

The lowest frequency T_{2g} modes depend on C_{44} as can be seen by their frequency variations in Fig. 1. We also consider the variation in their frequencies as a function of $C_{11}-C_{12}$ in Fig. 2 while varying either C_{11} or C_{12} one at a time. There is nearly perfect agreement in this figure between varying C_{11} or C_{12}. It is also very good for vibrations having other irreducible representations (not shown). This demonstrates that $C_{11}-C_{12}$ is a good choice for a parameter rather than C_{11} only or C_{12} only. Furthermore, the lowest frequency T_{2g} vibrations which come from the S_2^1 modes do not depend on the corresponding transverse sound speed $\sqrt{\frac{C_{11}-C_{12}}{2\rho}}$ as can be seen by the almost flat variation. The small variation observed near the value of gold is due to the anticrossing between the two lowest frequency T_{2g} branches. While the lowest branch is associated with the S_2^1 mode, the next upper one comes from T_3^1 modes. Had a less anisotropic material been chosen, this anticrossing pattern would have been less pronounced. Still, as will be discussed later, neglecting the mixings between these branches is a reasonable choice in many cases.

In both cases, the mode-dependent isotropic approximation is obtained by satisfying $C_{44}=\frac{C_{11}-C_{12}}{2}$. The displacements associated with the mode-dependent isotropic approximations can be constructed using symmetry arguments[18,11] from the $S_{2,m}$ displacements. $S_{2,0}$ and $\frac{S_{2,2}+S_{2,-2}}{\sqrt{2}}$ are two orthonormal E_g modes and $\frac{S_{2,2}-S_{2,-2}}{\sqrt{2}}$, $S_{2,1}$, and $S_{2,-1}$ are the three T_{2g} orthonormal modes. As has been shown,[17] the key parameter for the calculation of the S_2^1 modes is the transverse isotropic sound speed although the longitudinal one has also a very small contribution. Choosing the isotropic longitudinal sound speed is not critical also due to the fact that the quasilongi-

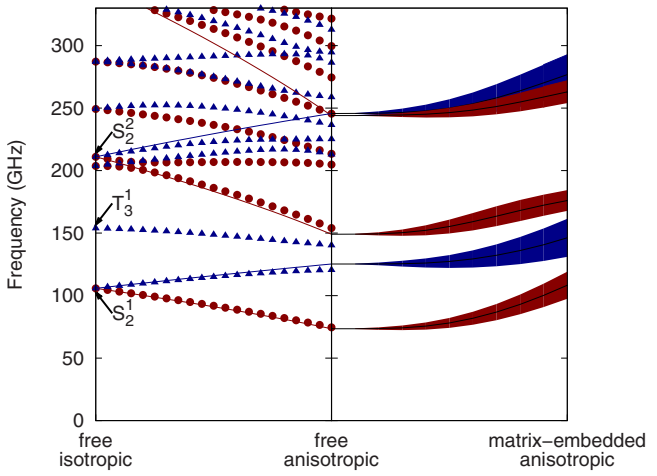

FIG. 3. (Color online) Left: variation in the frequencies using RUS (symbols) and Lamb with mode-dependent sound speeds (lines) when linearly varying the C_{ij} from isotropic to anisotropic gold. Radius $R=5$ nm. Right: matrix-induced broadening and frequency shift of the same modes. $v_L=\alpha\times 5020$ m/s, $v_T=\alpha\times 3010$ m/s, and $\rho=\alpha\times 2.97$ g/cm^3 for the matrix and the abscissa α is varied from 0 to 1 so as to reach the same value as in Ref. 16.

tudinal sound speed does not vary much with the propagation direction in gold. As a result, we simply used the 3D-averaged longitudinal sound speed as in previous works. This value is also the most appropriate one for an isotropic approximation of the breathing modes S_0 as has been already shown.[12]

III. APPLICATION

A. Free gold nanocrystals

Now the calculation of the eigenfrequencies of the modes coming from the spheroidal quadrupolar vibrations (S_2^1) for a sphere made of a material with cubic elasticity is separated into two isotropic problems which can each be solved exactly. The result of such calculations for a gold sphere are presented in the left part of Fig. 3 together with RUS calculations for varying anisotropy by using $C_{ij}(x)=C_{ij}^{iso}+x(C_{ij}^{ani}-C_{ij}^{iso})$ with $0\leq x\leq 1$, x being the abscissa, C^{iso} being the isotropic gold stiffness tensor obtained from the 3D-averaged sound speeds, and C^{ani} being the anisotropic one. The agreement between both kinds of calculations for the lowest three approximated branches is very good. The small deviation from the lowest frequency T_{2g} branch close to the "free anisotropic" limit can be attributed to the fact that the mixing with the next T_{2g} branch coming from T_3^1 is taken into account only in the RUS calculation. This mixing has not yet been observed experimentally (it should manifest as a splitting and intensity sharing between both branches). But even in that case, the frequency provided by the modified Lamb approach can be seen as a good approximation of the position of the expected Raman peak. As a result, this approach provides a simpler description of the vibrations which is quite suitable to interpret all the currently available experimental results for free nanocrystals.

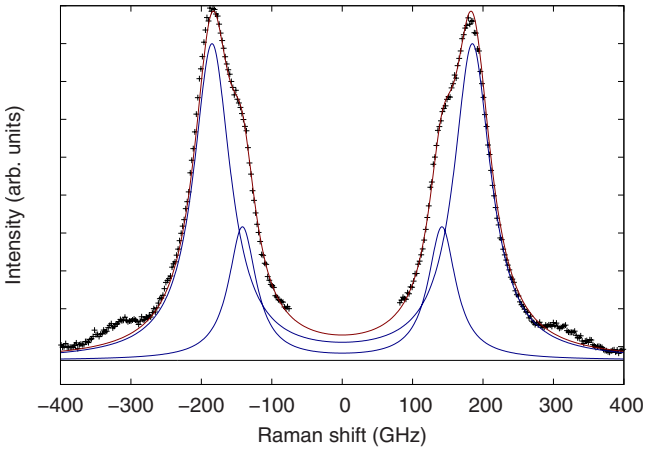

FIG. 4. (Color online) Low-frequency Raman spectrum for matrix-embedded gold nanoparticles (crosses). The fit of the intense lowest frequency band by two Lorentzians and a constant background is shown with lines.

B. Matrix-embedded nanocrystals

Since the coupling with an embedding matrix can be taken into account for a system having spherical symmetry, the isotropic approximations presented before for free nanocrystals can be extended to calculate the broadening and frequency shifts due to a surrounding matrix. In the following, we focus on calculations using the pseudomodes obtained with the complex frequency model (CFM).[12] Other models such as the core-shell model (CSM) (Ref. 12) would be more suitable for the calculation of Raman spectra but will not be considered here as we focus only on the positions of the Raman bands. Details about the validity of the CFM approach using the isotropic approximations are presented in Appendix.

CFM calculations are presented in Fig. 3 and compared to the experimental spectra of gold nanocrystals in Fig. 4 and Ref. 16. Figure 4 shows the Raman spectra of matrix-embedded gold nanocrystals. Details about the sample preparation and the spectra acquisition are the same as those presented in Ref. 16 with a 64 h annealing at $T=455$ °C. Figure 4 focuses on the intense lowest frequency peak which has been decomposed into a low-frequency E_g Lorentzian [position 141.6 ± 0.7 GHz, full width at half maximum (FWHM) 47.5 ± 1.9 GHz] and a higher frequency T_{2g} one (position 184.9 ± 0.4 GHz, FWHM 63.7 ± 1.2 GHz).

Figure 3 (right) presents the evolution from free to matrix-embedded gold nanocrystals by varying the parameters describing the matrix (mass density and longitudinal and transverse sound speeds). As discussed before, the calculations are expected to be accurate only for the lowest E_g and T_{2g} branches but higher frequency branches are shown as well for completeness. We used the parameters for the matrix which were measured by Brillouin scattering in previous works.[5,16] On the right-hand side of Fig. 3, the frequency of the E_g branch reaches 108.3 GHz (FWHM 21.7 GHz) while the T_{2g} one reaches 146.2 GHz (FWHM 30.4 GHz). While going from free to matrix-embedded nanoparticles, the ratio of the E_g and T_{2g} frequencies, which does not depend on the

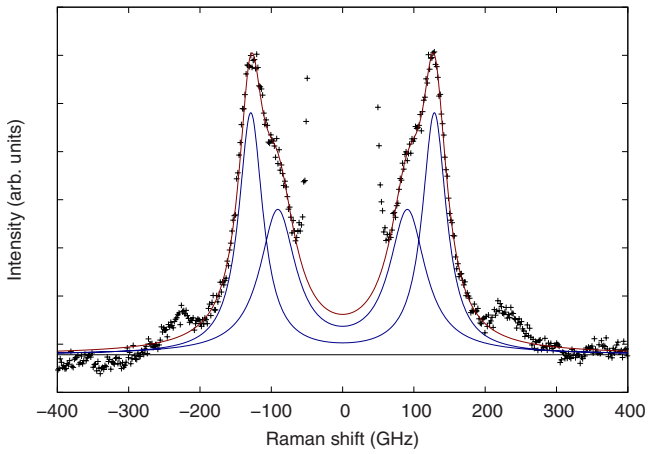

FIG. 5. (Color online) Low-frequency Raman spectrum for matrix-embedded copper nanoparticles (crosses). The fit of the intense lowest frequency band by two Lorentzians and a constant background is shown with lines.

size of the nanocrystals, changes from 0.59 to 0.74. Both values are in very good agreement with the experimental results presented here (ratio 0.77) and in Ref. 16 for embedded gold nanocrystals[16] as well as for free gold nanocrystals (ratio 0.62 in Ref. 19). This good agreement strongly supports the validity of the calculations based on the CFM and using the isotropic approximations obtained for the free spheres. Moreover, it enables the accurate determination of the size of the nanocrystals using the inverse proportionality of the eigenfrequencies with the diameter of the sphere.

A similar procedure was used to check the validity of our approach with matrix-embedded copper nanoparticles since copper crystallizes in a cubic structure too. Red Cu glasses were produced in a similar fashion to the Au-based glasses described in Ref. 16. By annealing near the glass transition temperature an initially transparent sodo-silicate glass containing minute quantities of both Cu_2O and SnO, nanometric clusters of metallic copper are formed. Based on a Maxwell Garnett description, the volume content of Cu under the form of nanoparticles is estimated as 10^{-5}. Similar values are expected for the previous gold samples. Low-frequency Raman spectra were recorded using a laser excitation close to the surface-plasmon resonance maxima ($\lambda=561$ nm for Cu instead of $\lambda=532$ nm for Au). Due to the observed splitting of the lowest frequency band, it is deduced that a substantial fraction of the formed Cu nanoparticles are monodomain nanocrystals. The density of the embedding glass is $\rho=2.43$ g cm^{-3} and the longitudinal and transverse sound velocities are, respectively, $v_L=5800$ m/s and $v_T=3510$ m/s, as determined from Brillouin spectroscopy. Note that these matrix parameters differ from those of the Au sample ($\rho=2.97$ g cm^{-3}, $v_L=5020$ m/s, and $v_T=3010$ m/s).

The mass density and C_{ij}'s for copper were obtained from Ref. 20. For free monodomain copper nanocrystals, the calculated ratio of the E_g to T_{2g} frequencies is 0.56 and it increases to 0.66 when embedded in the corresponding matrix. The ratio deduced from the fit presented in Fig. 5 is 0.71.

It should be noted that, as clearly demonstrated elsewhere,[19] multiply-twinned particles also contribute to the Raman spectra in the same frequency range through a broader peak. The broadening of the E_g and T_{2g} peaks for matrix-embedded nanocrystals prevents the clear identification of this additional contribution and therefore it is not possible to reliably fit it. However, by not taking it into account, the positions of the E_g and T_{2g} peaks are not very accurate which may explain the disagreements between the calculated and fitted ratios. For the same reason, the fitted intensities and widths of both peaks are seriously affected by the presence of such a third contribution. It is therefore important to restrict the usage of the fitting procedure used in this work to obtain only relatively accurate positions for the E_g to T_{2g} peaks. These should of course not depend strongly on the exact shape of the peaks (Lorentzian or Gaussian, for example).

Finally, an additional small peak at higher frequency can be seen in the spectra presented in Figs. 4 and 5. Within the isotropic approximation, this peak was assigned to the S_2^2 degenerated modes.[5] In the view of Fig. 3, i.e., accounting for the elastic anisotropy and the embedding matrix, this peak may tentatively be assigned to either the E_g modes deriving from the S_2^3 vibrations or the T_{2g} modes deriving from the S_2^2 modes. Since the latter modes are known to have a very small surface deformation, their expected Raman scattering cross section is expected to be negligible. Therefore we assign this third small peak to the E_g modes deriving from the S_2^3 vibrations.

IV. CONCLUSION

We have demonstrated that full anisotropic calculations are often not required to interpret low-frequency Raman spectra from spherical nanoparticles with cubic elasticity. Instead, simpler isotropic calculations with properly chosen sound speeds can provide approximate but accurate frequencies for the most intense Raman-active vibrations and allow to take into account the medium surrounding the nanocrystals. Calculations have been successfully compared to experimental results for the case of monodomain gold and copper nanoparticles in a glass matrix having isotropic elasticity. While the effect of the elastic anisotropy on the frequencies of the free vibrations was already known, the present work demonstrates the measurable impact it also has on the frequency splittings and the broadenings of the pseudomode for matrix-embedded nanoparticles. Such is important for a reliable size evaluation of nanoparticles from their low-frequency Raman spectra.

ACKNOWLEDGMENTS

We acknowledge Serge Etienne for providing some of the samples used in this work. Part of his work has been carried out within the FeNoPtiχ Project No. ANR-09-NANO-023 funded by the French National Agency (ANR) in the frame of its 2009 program in Nanosciences, Nanotechnologies and Nanosystems (P3N2009). D.B.M. acknowledges support from NSERC.

APPENDIX: VALIDITY OF THE CFM USED WITH THE ISOTROPIC APPROXIMATIONS

Let us consider a gold sphere of radius R_0. In order to apply the CFM approach to the case of spherical nanocrystals having anisotropic elasticity, we have to check that the displacement fields originally used in the isotropic CFM case are still approximate solutions of the wave equation for the anisotropic system for $r<R_0$ provided the correct C_{ij}'s are used.

Without any loss of generality, let us first consider the E_g modes similar to $S_{2,0}(m=0)$. We already know that the isotropic approximation presented before is valid for the lowest two E_g modes. We write the frequencies of these modes as $\nu_1=\frac{A}{R_0}$ and $\nu_2=\frac{B}{R_0}$ with $A<B$ in the following. This isotropic approximation is valid whatever the radius of the gold sphere and in particular for radii $R>R_0$. For a given frequency $\nu<\frac{A}{R_0}$, let us consider two particular spheres of radii $R_A=\frac{A}{\nu}$ and $R_B=\frac{B}{\nu}$ so that the first E_g mode of the first particle and the second E_g mode of the second particle have the same frequency ν. In the isotropic approximation, these $S_{2,0}$ displacements are linear combinations of two terms: $\vec{u}_L=\vec{\nabla} j_2(k_L r)P_2(\cos\theta)e^{i\omega t}$ and $\vec{u}_T=\vec{\nabla}\times\vec{\nabla}[\vec{r} j_2(k_L r)\times P_2(\cos\theta)]e^{i\omega t}$, where j_ℓ and P_ℓ are the spherical Bessel functions of the first kind and the Legendre polynomials, respectively, and $\omega=k_L v_L=k_T v_T$. Since two independent linear combinations of the same fields ($\vec{u}_L$ and $\vec{u}_T$) are approximate solutions of the wave equation, each field is an approximate solution too for $r<R_0$. Therefore we have checked that it is possible to apply the CFM approach in the frequency domain $\nu<\nu_1$.

The matrix often increases the pseudomode frequencies up to roughly 50% (i.e., roughly $\frac{\nu_1+\nu_2}{2}$) in the case of a very hard and dense matrix. We want to apply the CFM in that frequency range too. The fact that the calculations are also valid for $R<R_0$ is of no use here because it only demonstrates that the $S_{2,0}$ displacement field is a good approximation for the core of the sphere but nothing is known close to $r=R_0$. While we cannot extend this proof to $\nu>\nu_1$, we cannot prove either that this approximation fails very quickly when increasing ν above ν_1. For T_{2g} modes, the situation is also more problematic because the branch coming from S_2^2 mixes significantly with other T_{2g} branches coming from S_4^1, T_5^1, and S_6^1. Despite these limitations, applying the CFM can be useful at least as a rough estimation of the pseudomodes frequencies.

*lucien.saviot@u-bourgogne.fr
†daniel.murray@ubc.ca

[1] D. A. Weitz, T. J. Gramila, A. Z. Genack, and J. I. Gersten, Phys. Rev. Lett. **45**, 355 (1980).
[2] M. Fujii, T. Nagareda, S. Hayashi, and K. Yamamoto, Phys. Rev. B **44**, 6243 (1991).
[3] M. Fujii, T. Nagareda, S. Hayashi, and K. Yamamoto, Phys. Rev. B **52**, 14273 (1995).
[4] G. Bachelier and A. Mlayah, Phys. Rev. B **69**, 205408 (2004).
[5] S. Adichtchev, S. Sirotkin, G. Bachelier, L. Saviot, S. Etienne, B. Stephanidis, E. Duval, and A. Mermet, Phys. Rev. B **79**, 201402 (2009).
[6] H. Lamb, Proc. London Math. Soc. **s1-13**, 189 (1881).
[7] V. A. Dubrovskiy and V. Morochnik, Izv., Acad. Sci., USSR, Phys. Solid Earth **17**, 494 (1981).
[8] D. B. Murray and L. Saviot, Phys. Rev. B **69**, 094305 (2004).
[9] W. M. Visscher, A. Migliori, T. M. Bell, and R. A. Reinert, J. Acoust. Soc. Am. **90**, 2154 (1991).
[10] E. Mochizuki, J. Appl. Phys. **63**, 5668 (1988).
[11] H. Oda, J. Hirao, I. Suzuki, W. M. Visscher, and O. L. Anderson, Geophys. J. Int. **118**, 555 (1994).
[12] L. Saviot and D. B. Murray, Phys. Rev. B **79**, 214101 (2009).
[13] S. M. Hasheminejad and M. Maleki, Acoust. Phys. **54**, 168 (2008).
[14] N. Zuckerman and J. R. Lukes, Phys. Rev. B **77**, 094302 (2008).
[15] E. Duval, Phys. Rev. B **46**, 5795 (1992).
[16] B. Stephanidis, S. Adichtchev, S. Etienne, S. Migot, E. Duval, and A. Mermet, Phys. Rev. B **76**, 121404 (2007).
[17] L. Saviot and D. B. Murray, Phys. Rev. B **72**, 205433 (2005).
[18] T. Kahan, R. Jancel, R. Lacroix, and H. Poulet, *Théorie des Groupes en Physique Classique et Quantique* (Dunod, Paris, 1972), Vol. 3.
[19] H. Portalès, N. Goubet, L. Saviot, P. Yang, S. Sirotkin, E. Duval, A. Mermet, and M.-P. Pileni, ACS Nano **4**, 3489 (2010).
[20] C. Kittel, *Introduction to Solid State Physics*, 7th ed. (Wiley, New York, 1996).